SANS Study on the Effect of Lanthanide Ions and Charged Lipids on the Morphology of Phospholipid Mixtures

Mu-Ping Nieh,*† Charles J. Glinka,* Susan Krueger,*¶ R. Scott Prosser,‡ and John Katsaras§

*Materials Science and Engineering Laboratory, National Institute of Standards and Technology, Gaithersburg, Maryland 20899, †Department of Materials Science, The Pennsylvania State University, University Park, Pennsylvania 16802, and ‡Department of Chemistry and Liquid Crystal Institute, Kent State University, Kent, Ohio 44242 USA; and §National Research Council, Steacie Institute for Molecular Sciences, Neutron Program for Material Research, Chalk River Laboratories, Chalk River, Ontario K0J 1J0, Canada

ABSTRACT The structural phase behavior of phospholipid mixtures consisting of short-chain (dihexanoyl phosphatidylcholine) and long-chain lipids (dimyristoyl phosphatidylcholine and dimyristoyl phosphatidylglycerol), with and without lanthanide ions was investigated by small-angle neutron scattering (SANS). SANS profiles were obtained from 10°C to 55°C using lipid concentrations ranging from 0.0025 g/ml to 0.25 g/ml. The results reveal a wealth of distinct morphologies, including lamellae, multi-lamellar vesicles, unilamellar vesicles, and bicellar disks.

INTRODUCTION

The bilayered micelles (known as bicelles) and related phospholipid mixtures are important magnetically alignable model membrane systems for solid-state NMR studies of membrane peptides and proteins (Sanders and Prosser, 1998) and, more recently, for high-resolution NMR studies of membrane peptides (Vold et al., 1997; Luchette et al., 2002). Though a wide variety of formulations exist, these bilayered mixtures have in common a short-chain phospholipid (typically, dihexanoyl phosphatidylcholine (DHPC)) and one or more long-chain phospholipids (typically, dimyristoyl phosphatidylcholine (DMPC) and a negatively charged lipid such as dimyristoyl phosphatidylglycerol (DMPG)). The short-chain lipids greatly facilitate alignment of bilayers and are critically important in the lanthanide and non-lanthanide doped bilayers. The phase boundaries of the magnetically alignable bilayers can often be extended by the addition of DMPG, which also serves to represent the negatively charged lipid content, typical of biomembranes (Losonczi and Prestegard, 1998).

The bilayered mixtures align in a magnetic field, **B**, with the bilayer normal, $\mathbf{n} \perp \mathbf{B}$ above a certain molar ratio of long-chain to short-chain lipid, q (usually $q > 2.5$) and certain temperature (>35°C) (Sanders and Landis, 1994; Sanders et al., 1994). The viscosity of the mixtures also abruptly increases above the transition temperature (~30°C). Uniform alignment of the samples can significantly improve the spectral resolution compared with powder patterns from randomly dispersed samples in solid-state NMR. The magnetically alignable bilayered mixtures were thought to be discoidal (Sanders and Schwonek, 1992) with the long-chain lipids sequestered primarily to the planar surface of the bilayered disks and the short-chain lipids coating the edge of the disks. We refer to this structure as bicellar disk in this paper. Although widely accepted in public, the discoidal structure has not been verified experimentally.

For smaller values of molar ratio, q ($0.2 < q < 1$), NMR and small-angle neutron scattering (SANS) studies support the bicellar disk structural model for negatively charged mixed lipid bilayers (Luchette et al., 2002). The disks are small in dimensions and thus exhibit fast tumbling in the solution and cannot be magnetically aligned. In this case, the bicellar disks serve as ideal substrates for the study of membrane peptides using high-resolution solution NMR, for the fast tumbling motion averages out the anisotropic interactions and yields spectra with finer line width, i.e., a better resolution.

In many cases, it is advantageous for both NMR and small-angle scattering to employ a magnetically alignable model membrane, in which **n** is parallel with **B** (Ulrich and Watts, 1993). This also facilitates the application of other spectroscopic techniques (for example, Fourier transform infrared (FTIR) or fluorescence anisotropy), which make use of oriented transition dipole moments. Parallel alignment can be achieved by the addition of some particular lanthanide ions such as Yb^{3+} or Tm^{3+} (Prosser et al., 1996; 1998a,b,c; Katsaras et al., 1997). Our previous SANS study on these lanthanide-doped lipid mixtures indicated that this magnetically alignable phase adopts lamellar structure with defects in the form of pores that perforate the bilayers (Nieh et al., 2001). In comparison with the non-lanthanide doped bilayers, although both systems exhibit similar temperature-dependent viscosity trends and local (long-chain) lipid order parameter profiles, there is no direct evidence that the doped bilayers form the same structural phases at the corresponding lipid concentrations and temperatures.

Because the application of these bilayered mixtures depends on their morphologies, the understanding of the structural phases of mixed lipid bilayers and related systems may help optimize their use in various techniques (i.e., high-

Submitted October 4, 2001, and accepted for publication January 10, 2002.

Address reprint requests to Dr. Mu-Ping Nieh, National Institute of Standards and Technology, E20, Bldg. 235, Gaithersburg, MD 20899. Tel.: 301-975-4899; Fax: 301-921-9847; E-mail: muping.nieh@nist.gov.

0006-3495/02/05/2487/12 $2.00

resolution NMR of weakly aligned water soluble proteins and solid-state NMR and SANS of membrane peptides in aligned media). Recently, three phases (isotropic, bicellar, and lamellar) were inferred for the neutral DMPC/DHPC system on the basis of ^{31}P and ^{1}H solid-state NMR experiments as a function of temperature and q (Raffard et al., 2000). Complementary methods, such as small-angle x-ray or neutron scattering are useful for identifying the various structural phases and the existence of long range order. A small-angle x-ray scattering (SAXS) study of the neutral DMPC/DHPC membrane indicated the presence of various morphologies as the temperature and total lipid concentration varied (Bolze et al., 2000). However, due to a lack of data at small scattering angles, the authors could not unambiguously identify the morphologies.

This paper presents recent SANS results, which elucidate the morphological and structural phases of the neutral (DMPC/DHPC) and negatively charged (DMPC/DHPC/DMPG) and lanthanide-doped lipid bilayered mixtures (DMPC/DHPC/DMPG/Tm^{3+}) at various concentrations and temperatures. From these data, a structural phase diagram has been constructed for each system to provide a better understanding of the surface charge effect on morphology.

MATERIALS AND METHODS

Materials

DMPC, DHPC, and DMPG were purchased from Avanti Polar Lipids (Alabaster,AL) whereas thulium chloride hexahydrate (99.99%), $TmCl_3 \cdot 6H_2O$, was obtained from Aldrich Chemicals (Milwaukee, WI). All chemicals were used without further purification.

Sample preparation

Three distinct lipid mixtures were investigated using SANS: 1) DMPC/DHPC in a molar ratio of 3.2/1, denoted simply as PC, 2) DMPC/DHPC/DMPG (molar ratio: 3.2/1.0/0.21), denoted as PC/PG, and 3) a thulium-doped mixture, DMPC/DHPC/DMPG/Tm^{3+} (molar ratio: 3.2/1.0/0.21/0.043) denoted as PC/PG/Tm. Tm^{3+} possesses the largest positive magnetic anisotropy of the lanthanide series, making it an ideal choice for magnetic alignment. It should also be noted that the amount of Tm^{3+} used in PC/PG/Tm was only 10% of that employed in an earlier neutron diffraction study (Katsaras et al., 1997).

Deuterium oxide (99.9%, Cambridge Isotope Co.) was used for all lipid/water mixtures, and the total lipid concentration, c_{lp}, was varied from 0.0025 to 0.25 g/ml for each series of mixtures. Samples were prepared beginning with the most concentrated mixtures (c_{lp} = 0.25 g/ml), which were initially vortexed at temperatures between 40°C and 50°C and then cooled to ~10°C to remove air bubbles. This procedure was repeated until the mixture was homogeneous. Samples in each series were prepared from the most concentrated samples by diluting to the desired c_{lp} and storing at 10°C. Measurements were performed in order from 10°C, 25°C, 35°C, 45°C, and 55°C, respectively.

SANS instrument and data reduction

SANS experiments were performed on the NG3 30m SANS instruments located at the National Institute of Standards and Technology (NIST) Center for Neutron Research (Gaithersburg, MD). For the present experiments we employed neutrons of wavelength (λ) 6 Å and a wavelength spread ($\Delta\lambda/\lambda$) of 15% (full width at half-maximum). To obtain a wide range of scattering vectors, two sample-to-detector distances (SDDs) were used, resulting in an effective Q range of between 0.004 $Å^{-1}$ and 0.3 $Å^{-1}$. The scattering vector, $\mathbf{Q}$, is defined as $(4\pi/\lambda)(\sin\theta)$, where θ is the scattering angle between the incident and the scattered neutron beams. The time-averaged Q-dependent scattering intensity, I, is the spatial Fourier transform of density and concentration fluctuations and is collected by a two-dimensional detector. The two-dimensional raw data were corrected for ambient background and empty cell scattering, and were put on an absolute scale (scattering cross section per unit volume) by a direct measurement of the incident neutron flux on the sample (Glinka et al., 1998). The corrected data were then circularly averaged to yield the one-dimensional intensity distribution, $I(Q)$. The incoherent scattering intensity was determined from the plateau of the high-Q data.

RESULTS

Four types of SANS patterns representative of different morphologies were observed for the three series of phospholipid mixtures studied. Some of the SANS profiles show mixtures of these prototypical patterns. Through detailed analysis of each pattern, the structures have been identified to be bicellar disk, perforated lamella, unilamellar vesicle (ULV), and multilamellar vesicle (MLV).

Bicellar discoidal morphology

The bicellar disk morphology (Vold and Prosser, 1996) can be approximated with a core-shell-disk model, where the core and shell of the disk consist of the hydrophobic tails and hydrophilic headgroups of the lipid molecules, respectively. A detailed description and derivation for the core-shell-disk model is given in the Appendix. A characteristic feature of this model is a Q^{-2} dependence of $I(\mathbf{Q})$ in the vicinity of $\pi/(L + 2t) > Q > 2\pi/2R$, when the disk radius, R (150 Å), is much larger than the disk thickness, $L + 2t$ (48 Å), where L and t are the hydrophobic and hydrophilic thicknesses. This feature is seen in the SANS pattern obtained for the sample with the lowest lipid concentration (c_{lp}) = 0.0025 g/ml at 10°C in PC/PG/Tm mixture (Fig. 1). Good agreement of the best-fit result (solid line in Fig. 1) with the data supports this choice of model.

As c_{lp} increases, bicelles begin to interact resulting in a broad interparticle interference peak in the SANS profiles. Fig. 2 shows for PC/PG mixtures that the peak position, Q_{peak}, shifts toward lower Q upon dilution. This peak corresponds to an interparticle spacing, D, which is $\sim 2\pi/Q_{peak}$. The SANS profiles for the lowest c_{lp} (0.0025 g/ml) samples of the PC/PG and PC/PG/Tm mixtures are almost identical for $Q > Q_{peak}$ (compare Figs. 1 and 2) except for this interparticle interference peak. Thus, we conclude that the PC/PG sample with c_{lp} = 0.0025 g/ml also has the bicellar discoidal morphology. The peak appears in the data for PC/PG samples (c_{lp} = 0.0025 g/ml) likely due to its higher surface charge density, which causes a more regular inter-

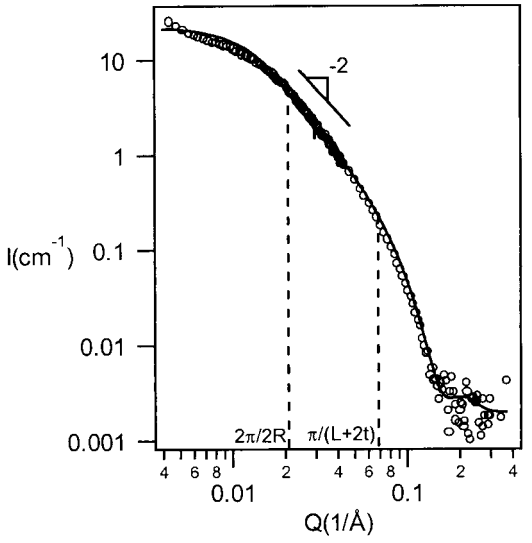

FIGURE 1 The SANS data (○) and best-fitting result (——) using the bicellar core-shell discoidal model (Eq. 1) for the PC/PG/Tm sample with $c_{lp} = 0.0025$ g/ml at $T = 10$°C (the best-fit parameters are $R = 150 \pm 15$ Å, $L = 32 \pm 3$ Å, and $t = 8 \pm 1$ Å).

particle spacing. Because the assumption of randomly oriented disk breaks down when the bicelles began to interact, the core-shell-disk model cannot be used to fit the data from more concentrated samples. Nevertheless, some important information can be revealed by plotting the interparticle

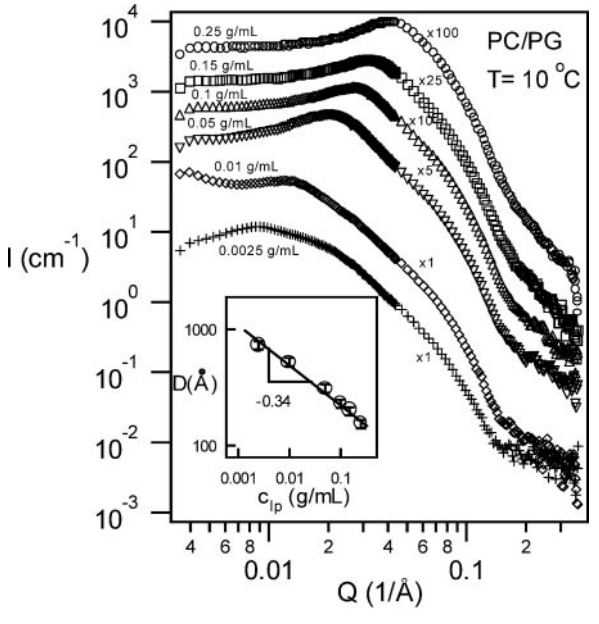

FIGURE 2 SANS results for the PC/PG series of mixtures at $T = 10$°C. The scattering data have been scaled with the arbitrary factors indicated to better distinguish the curves. The inset is the plot of the d-spacing, D, as a function of lipid concentration, c_{lp}. The fitted line has a slope of -0.34 ± 0.02, representing a three-dimensional swelling.

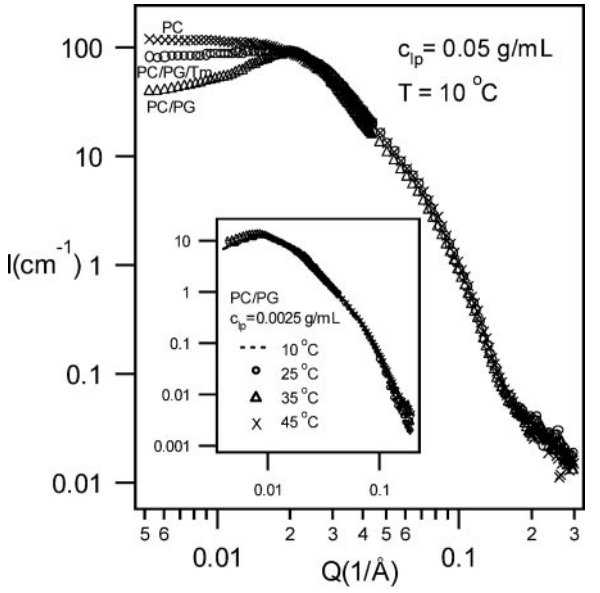

FIGURE 3 Comparison of SANS profiles of the PC, PC/PG, and PC/PG/Tm samples with $c_{lp} = 0.05$ g/ml at 10°C. The sharpness of the peak, reflecting the interparticle interference, decreases in the sequence of PC/PG, PC/PG/Tm, and then PC. The inset shows the SANS data for the PC/PG sample with $c_{lp} = 0.0025$ g/ml at various temperatures from 10°C to 45°C. The data collapse onto a single curve indicating that the morphology does not change.

spacing, D, as a function of c_{lp} (the inset of Fig. 2). A linear relationship in a log-log plot is obtained with a slope of -0.34 ± 0.02. Because $D \propto c_{lp}^{-1/d}$, where d is the dimensionality, the mixtures exhibit three-dimensional swelling at 10°C. Moreover, the continuous linearity throughout the whole range of examined c_{lp} implies that no aggregation or fragmentation of the bicellar disks occurs upon dilution. Therefore, we conclude that the morphology of the PC/PG mixture remains that of bicellar disks at 10°C for all of lipid concentrations examined (from 0.0025 to 0.25 g/ml). Note that the SANS data for $c_{lp} = 0.0025$ g/ml in the PC/PG mixture did not vary with T (from 10°C to 45°C), as shown in the inset of Fig. 3, indicating that the bicellar morphology is quite stable at such low c_{lp}.

The SANS patterns for the samples with $c_{lp} \geq 0.05$ g/ml for all three series of mixtures exhibited the morphology of bicellar disks at 10°C. The system with the higher charge density yielded lower intensity at the low Q regime and a more prominent scattering peak because of the interparticle interference. This effect of charge density on the SANS profiles is more obvious for the lower c_{lp} samples. For instance, at highest c_{lp} (0.25 g/ml) and 10°C, the SANS results for the three mixtures are almost identical; however, for the samples with $c_{lp} = 0.05$ g/ml, the dependence of scattering curve on the charge density is clearly observed as shown in Fig. 3. Note that the charge density on the bicellar

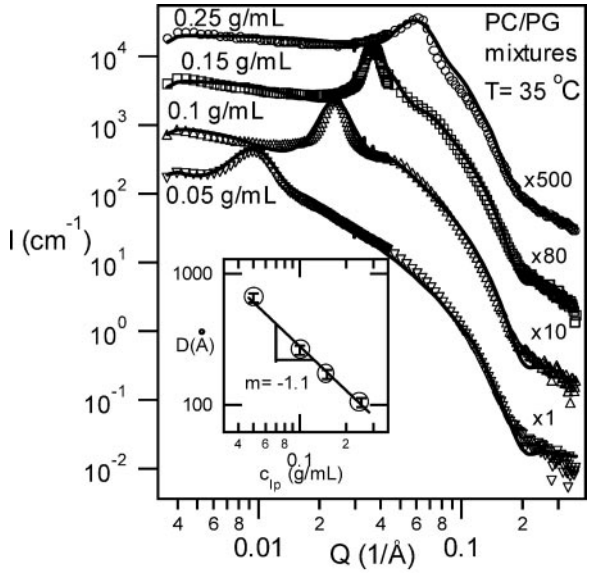

FIGURE 4 SANS results for the PC/PG series of mixtures at $T = 35$°C. The scattering data have been scaled by the arbitrary factors indicated to better distinguish the curves. The solid curves are the best-fit results from the lamellar model described in Appendix B (Eq. 4). The best-fit parameters are listed in Table 1. The inset is the plot of the d-spacing, D, as a function of lipid concentration, c_{lp}. The fitted line has a slope of -1.1 ± 0.1, indicating one-dimensional swelling.

TABLE 1 Best-fit parameters using the lamellar model for PC/PG mixtures with C_{lp} = 0.05–0.25 g/ml

c_{lp} (g/ml)	T (°C)	R_{lam} (Å)	D (Å)	σ_D (Å)	t (Å)*	L (Å)
0.25	35	68	106	37	10	24
0.15	35	150	172	48	7	25
0.1	35	260	265	75	8	23
0.05	35	5000	630	215	8	22
	45	5000	455	110	7	24

σ_D is the standard deviation of D. Through the fitting process, ρ_{phob}, ρ_{phil}, and $\rho_{solvent}$ remain constant according to literature reports or calculations with the values of -4.3×10^{-7}, 3.3×10^{-6}, and 6.38×10^{-6} Å^{-2}, respectively.

*Parameters were constrained to reasonable ranges acording to literature reports.

†Theoretically, a greater value is possible without altering the best-fit result, but the fit curve could be distorted for greater values due to the integration setting in our program. Thus, the value can be considered to be infinite.

disks decreases in the sequence of PC/PG, PC/PG/Tm, and PC.

Above 35°C, bicellar disks were no longer stable. Other scattering patterns were observed in these series of mixtures that have been identified as perforated lamellar (L), unilamellar vesicular (ULV), and multilamellar vesicle (MLV) structures; these are discussed in detail in the following sections.

Perforated lamellar morphology

As T increased to 35°C and above, the interparticle interference peak became more pronounced and shifted for PC/PG (Fig. 4) and PC/PG/Tm mixtures with $c_{lp} \geq 0.05$ g/ml. The sharpness of the peak indicates a more highly ordered and regularly spaced structure, typical of a lamellar phase. The most direct evidence for the lamellar structure comes from plotting the interparticle spacing, D, as a function of c_{lp} on a log-log plot (the inset of Fig. 4) yielding a line with a slope of -1.1 indicative of one-dimensional swelling.

These data are best described by a lamellar model with long-range order, i.e., an effectively infinite stack of lamellae (see Appendix). The model consists of finite-sized lamellae with hydrophobic cores and hydrophilic shells along with a Gaussian distribution for the interlamellar (interparticle) spacing, which strongly affects the intensity and the width of the peak. The parameters in Table 1 obtained from the fits give reasonable values for the bilayer thickness, $t_{bilayer}$, ranging from 38 Å to 44 Å, consistent with the result from null-contrast lipid mixtures in our previous study (Nieh et al., 2001). Note that the best fitting result for lamellar radius, R_{lam}, increases upon dilution, indicating that lamellae become more extended laterally.

For a homogeneous lamellar system, D can be calculated to be $t_{bilayer}/\phi_{lp}$, where ϕ_{lp} is the volume fraction of the lipid. In our case, the calculated D was always larger than $D = 2\pi/Q_{peak}$. This result suggests that the lipids occupy only ~60% of the individual lamellar surface area. Our previous SANS result on the aligned lamellae exhibited a monotonic decay followed by an intensity plateau with increased Q, when the incident neutron beam was parallel to the bilayer normal (in-plane scattering), indicative of the perforated structure, presumably pores (Nieh et al., 2001). The perforated defects are induced by adding the short-chain lipids, DHPC, which coat the edges of the pores to minimize the curvature energy.

For PC mixtures with $c_{lp} \geq 0.1$ g/ml, the transition from bicellar disks to perforated lamellae upon increasing T until 45°C (Fig. 5 *a*) is not as obvious as that of the PC/PG and PC/PG/Tm mixtures (Fig. 5 *b* and *c*) because of a more diffuse interlamellar interference peak. In fact, the transition from bicelles to lamellae occurred gradually upon increasing T. At 25°C, the scattering profile showed features of both bicelles and lamellae in all cases (Fig. 5, *a–c*). This is consistent with the reported viscosity behavior (Struppe and Vold, 1998), which began to increase abruptly around 23°C. The scattering pattern of PC mixtures at 45°C can be ascribed to a lamellar structure with a less regular spacing. The lamellar structure was almost completely established at 35°C for the PC/PG mixtures (Fig. 5 *c*). For the PC/PG/Tm mixtures, the lamellar peak approached to its equilibrium location at 35°C and then became sharper at 45°C (Fig. 5 *b*). However, for PC mixtures, not until $T = 45$°C did the

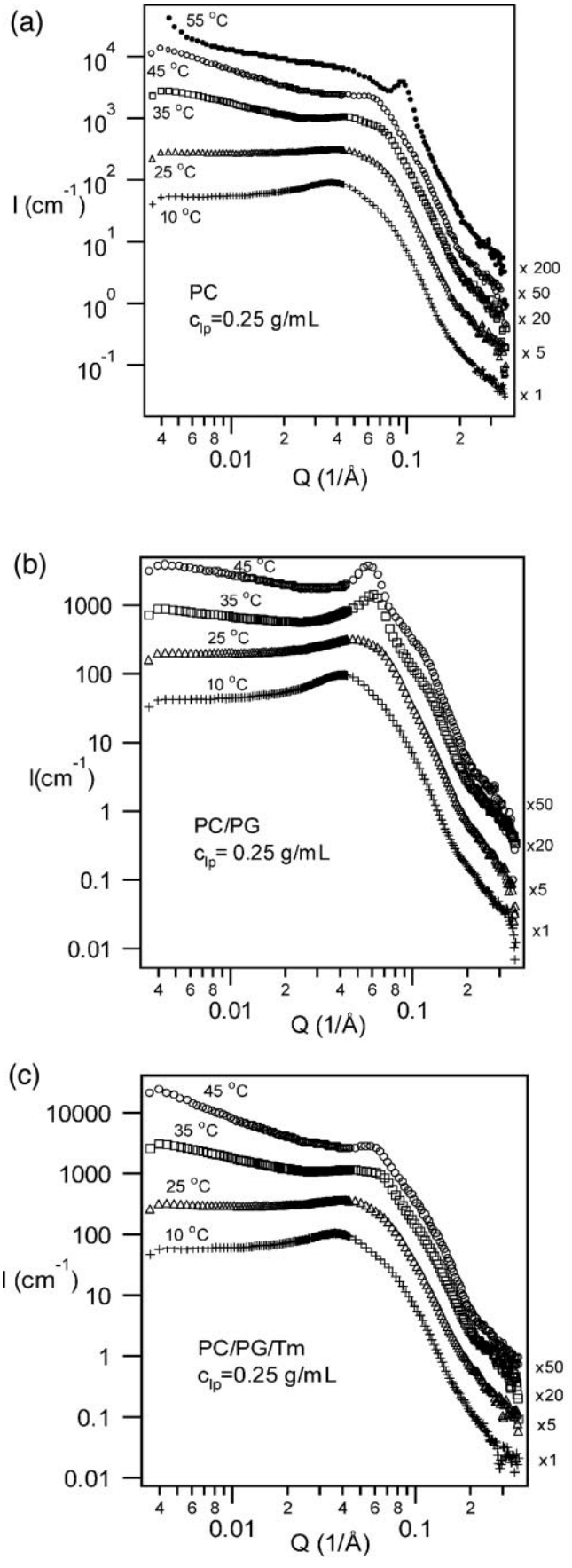

FIGURE 5 Example of temperature dependence of the samples with c_{lp} = 0.25 g/ml in PC (*a*), PC/PG (*b*), and PC/PG/Tm (*c*) series of mixtures. The SANS result shows a smooth phase transition from bicelle to lamella for all three series. The transition temperature is ~35°C.

lamellar peak reach to the same location as that in PC/PG or PC/PG/Tm mixtures, indicative of a non-sharp phase transition (Fig. 5 *a*).

In the case of the PC/PG mixture with c_{lp} = 0.05 g/ml (Fig. 6 *a*), the scattering pattern changed dramatically with an increase in T from 35°C to 45°C. Note that the interlamellar diffraction peak became sharper and shifted toward a higher value of Q at 45°C, and a second order peak became visible, indicative of a smaller but more regular interparticle spacing. The infinite stacked lamellar model can also fit these data well as shown in Fig. 6 *a* (the solid curve). Thus, this structure is denoted as the L_2 phase to distinguish it from the perforated lamellar phase. For c_{lp} = 0.01 g/ml in the PC/PG mixture, the value of bicellar interparticle peak, Q_{peak}, shifted continuously toward lower values of Q with increased T (Fig. 6 *b*), indicating a continuous increase in D (explained in the Discussion).

Unilamellar vesicular morphology

For the samples of the PC/PG/Tm series with $c_{lp} \leq 0.01$ g/ml and $T \geq 35$°C, yet another type of scattering curve, peaked at $Q = 0$ with weak secondary peaks at finite Q, was observed as shown in Fig. 7. The structure we find most consistent with these scattering curves is that of ULVs, which were modeled as polydispersed spherical shells (Appendix). This structure was identified in our previous study in the same range of c_{lp} and T for the lanthanide-doped mixtures (Nieh et al., 2001). Good agreement between the data and the best-fit result of this model, as shown in Fig. 7, supports the proposed structure. Note that the ULV was observed only in the PC/PG/Tm mixtures, and the best-fit shell radius, R_o, decreased with decreased c_{lp} (R_o = 186 ± 10 and 100 ± 10 Å for c_{lp} = 0.01 and 0.0025 g/ml, respectively).

Multilamellar vesicular morphology

Fig. 5 *a* shows that the SANS profile for PC mixtures of c_{lp} = 0.25 g/ml at high T (55°C) dramatically differs from those at other temperatures. This transition of the scattering pattern due to increased temperature was also observed in other samples of higher c_{lp} (from 0.01 to 0.25 g/ml, data not shown here). At 55°C, a peak was observed at $Q = 0.096 \pm 0.005$ $Å^{-1}$, corresponding to a D spacing of 66 ± 3 Å. The peak position did not vary with c_{lp}, indicating non-swelling upon dilution. The MLV structure has been reported in pure DMPC aqueous solutions (Laggner, 1994), and our experimental value of D agrees with the bilayer spacing of MLV

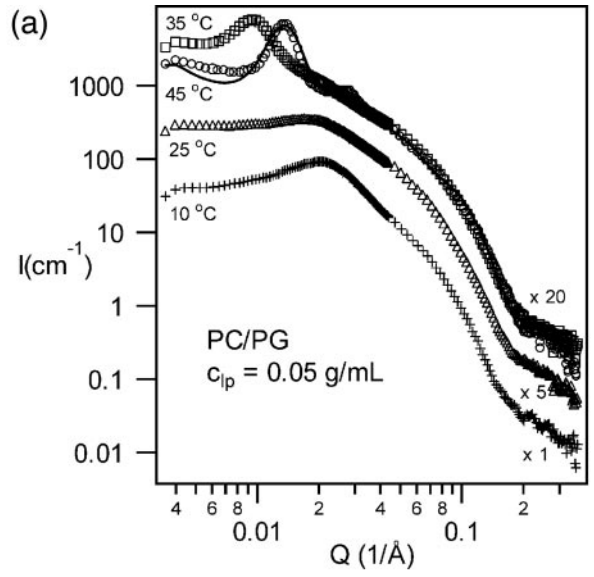

FIGURE 6 SANS results for the temperature dependence of the PC/PG series at c_{lp} of 0.05 (*a*) and 0.01 (*b*) g/ml. The scattering data have been scaled with the arbitrary factors indicated to better distinguish the curves. In *a*, the solid curve is the best-fitting result obtained with the lamellar model (Eq. 4) for the data at 45°C. The best-fit parameters are listed in Table 1. At this temperature a new, apparently lamellar, phase forms with a smaller, and better defined, average D-spacing. Note that the same scaling factor is applied to the data of 35°C and 45°C for comparison.

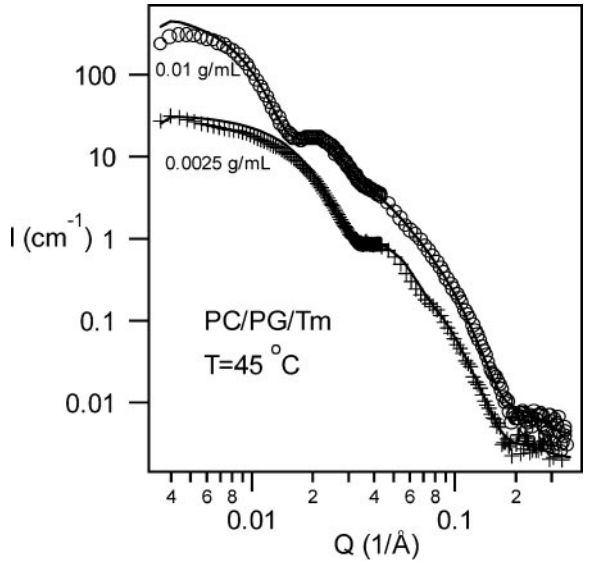

FIGURE 7 SANS data (○) and best-fitting results (——) for the PC/PG/Tm series at T = 45°C for both c_{lp} = 0.1 and 0.0025 g/ml using a poly-dispersed unilamellar vesicular (core-shell sphere) model (Eq. 5). The best-fit results for both c_{lp} values are in Appendix C.

for the pure DMPC system (Caffrey et al., 1991; Lohner et al., 1999). The sharpness of the peak (regular spacing) and invariance of the peak position with c_{lp} (non-swelling) are also consistent with the physical features of MLV; thus, the appearance of such a peak is strongly indicative of MLV. Recently, NMR studies on PC mixtures revealed that a fraction of DHPC was free from the liquid crystalline phase at low c_{lp} (Ottiger and Bax, 1998; Glover et al., 2001). An NMR result of labeled d_{22}-DHPC in a PC mixture (q = 4.5) also showed an increasing isotropic spectral component indicative of DHPC possibly forming a separate micellar phase at high T = 60°C (Sternin et al., 2001). If this were the case, the remaining DMPC-rich lipid mixture would be expected to adopt an MLV phase. Because pure DHPC micelles would be comparatively small, the SANS data mainly reflect the scattering from the MLVs. Because the SANS pattern characteristic of the MLV structure was observed only in PC mixtures, this section focuses on this series.

The SANS profiles show that the formation of MLV depends not only on T but also on c_{lp}. The lower the c_{lp}, the lower the transition temperature. For the PC samples with c_{lp} = 0.0025 g/ml, the MLV peak appeared in the SANS profiles and was fully developed at 25°C, and for c_{lp} = 0.01 g/ml, at 35°C (Fig. 8). At medium c_{lp} (0.05 g/ml), the MLV peak began to appear at 35°C (Fig. 8), and for higher c_{lp} (from 0.1 g/ml to 0.25 g/ml) the peak was observed only at 55°C (Fig. 5 *a*). This observation indicates that high T and low c_{lp} promote the formation of MLVs. A great change in the appearance of the samples was also found while the MLV formed. At 35°C, samples with c_{lp} = 0.01 g/ml and 0.05 g/ml underwent visible macroscopic phase separation, which was reported by Ottiger and Bax (1998). The bottom and major portion of the sample was a transparent aqueous solution, whereas the top lipid-rich layer was turbid foam. The SANS measurements were always made from the transparent aqueous solution. As a result, a dramatic intensity drop was observed from 25°C to 35°C for c_{lp} = 0.05 g/ml and from 10°C to 25°C for c_{lp} = 0.01

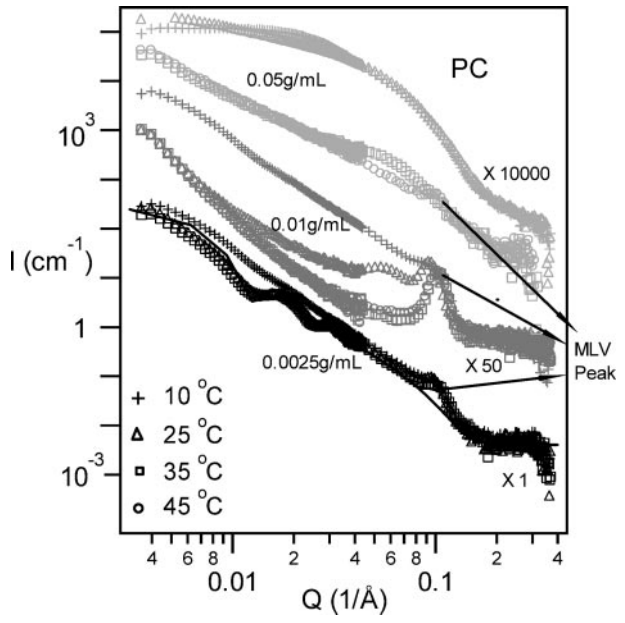

FIGURE 8 Temperature dependence of lower c_{lp} samples (from 0.0025 to 0.05 g/ml) in PC series of mixtures, where the scattering data have been re-scaled with an arbitrary factor for each set of c_{lp}. The solid line is the best-fit result for the sample of $c_{lp} = 0.0025$ g/ml at $T \geq 25$°C using the ULV model. These data show that the bicelle→MLV transition temperature decreases with decreased c_{lp}.

g/ml, indicative of less lipid in the transparent aqueous solution after the phase separation. For higher c_{lp} (from 0.1 g/ml to 0.25 g/ml), the samples became opaque at 55°C, when MLV peaks appeared in the scattering profiles. However, neither visible phase separation nor a clear intensity drop was observed.

Note that at $T \geq 25$°C, all the scattering data from the PC mixtures for $c_{lp} = 0.0025$ g/ml fell onto a single curve containing an MLV peak and several peaks in the lower Q regime ($Q < 0.04$ Å^{-1} in Fig. 8). These low-Q peaks can be characteristic of the scattering from ULVs as described in the Appendix. The best fit for the ULV model agrees with the data well, except in the vicinity of the MLV peak, yielding an outer radius of 275 ± 10 Å. This result indicates that either ULVs and MLVs coexisted in the system or this fitted radius was the average outermost shell radius of the MLV. The former scenario is very unlikely because this dimension is too large for the radius of the neutral or weakly charged ULVs at such low c_{lp} (Nieh et al., 2001). Thus, we infer that MLVs are the likely explanation for such a scattering pattern. The radius of MLVs in PC mixtures should have the same c_{lp} dependence as that of ULVs in PC/PG/Tm mixtures: the radius increasing with increased c_{lp}. Therefore, these low-Q peaks were not found for other more concentrated samples, because the peaks corresponding to MLV outermost radii were beyond the resolution of our instrument.

DISCUSSION

The SANS results are summarized in the structural phase diagrams in Fig. 9. Dramatic differences among them show a strong effect of surface charge on the structures. For the PC mixtures (Fig. 9 *a*), the symbol in each phase represents the dominant structure of that phase, because no clearly defined phase transition boundary was obtained, and the gray area shows where the phase separation or opaqueness in the samples occurs. Generally speaking, randomly oriented bicellar disks exist at high c_{lp} (~0.05–0.25 g/ml) and low T (10°C). Magnetically alignable lamellae occur in the range of high c_{lp} (~0.1–0.25 g/ml) and medium T (35°C and 45°C), and MLVs form at high T (55°C) or low c_{lp} (!0.0025–0.05 g/ml). Fig. 9 *b* shows the phase diagram for the PC/PG series of mixtures, where only two morphologies were verified: bicelles and lamellae. Although measurements were not taken for charged mixtures at higher T because of insufficient SANS time, the lamellar phase of PC/PG mixture was found very stable until 90°C for $q = 5$, consistent with the observation by Brunner et al. (2001). Another type of lamellae, L_2, was also observed at $c_{lp} = 0.05$ g/ml at 45°C. The exact morphology for $c_{lp} = 0.01$ g/ml above 25°C is not known yet. Compared with the PC mixtures, the phase transition boundaries are sharper. Fig. 9 *c* shows the structural phase diagram for the PC/PG/Tm series consisting of three morphologies, bicellar disks, perforated lamellae, and ULVs, consistent with the results of our previous study (Nieh et al., 2001).

Fig. 10 *a* compares the SANS profiles for three mixture (PC, PC/PG, and PC/PG/Tm) in addition to a PC lipid mixture doped with the same molar ratio of thulium (PC/Tm) previously reported by Nieh et al. (2001). All the SANS profiles are consistent with that of a lamellar phase, though there are some distinct scattering features of the respective mixtures. Note that the position of the peak, Q_{peak}, is independent of charge density and is relatively invariant with respect to the three mixtures (Q_{peak} is slightly higher for the PC mixtures), indicating that the average interparticle spacing remains relatively unaffected by the presence of charge in the system. However, the sharpness of the peak is clearly dependent on surface charge. As seen in the inset of Fig. 10 *a*, the PC/PG series exhibits the sharpest peak, indicating the most regular lamellar repeat spacing as a result of greater interlamellar repulsion and a corresponding higher surface charge density. The peak associated with the PC/Tm series is also sharp due to the surface charge from the association of Tm^{3+} ions (Prosser et al., 1998a,b). The negative charge imparted by the phosphatidylglycerol in the PC/PG/Tm is partially screened by the positively charged Tm^{3+} resulting in a less regular spacing between lamellae. Finally, in the case of the neutral membrane system, the lamellar peak is least well defined. X-ray scattering results of a PC sample with $c_{lp} = 0.3$ g/ml also

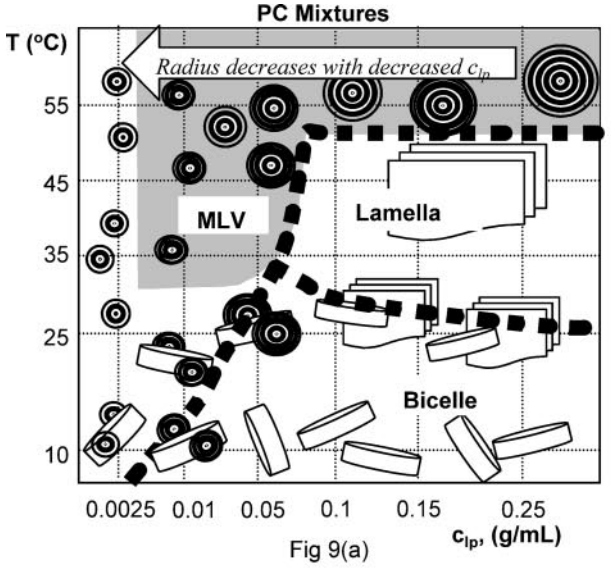

Fig 9(a)

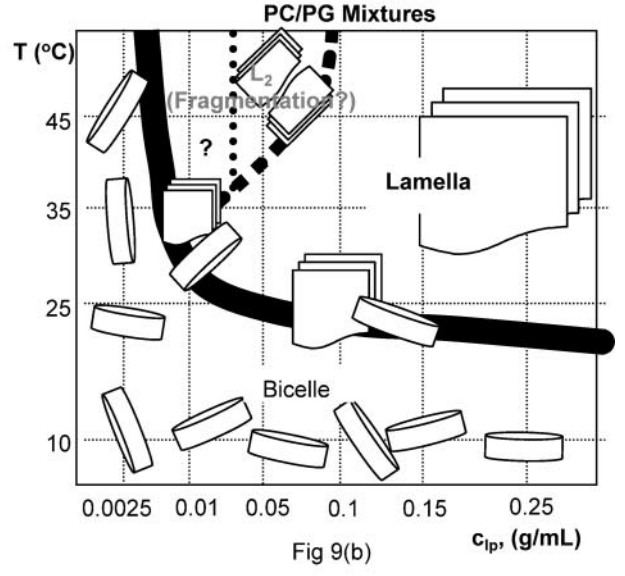

Fig 9(b)

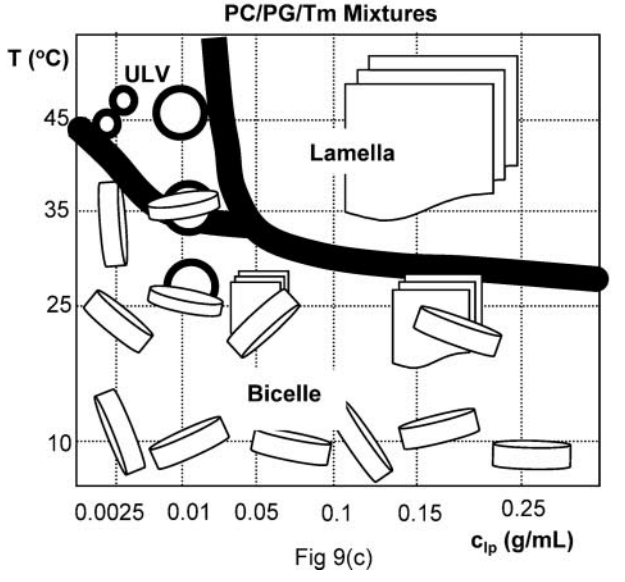

Fig 9(c)

FIGURE 9 Structural phase diagrams for PC (*a*), PC/PG (*b*), and PC/PG/Tm (*c*) series of mixtures. The gray region shows where some degree of macroscopic phase separation was visually observed.

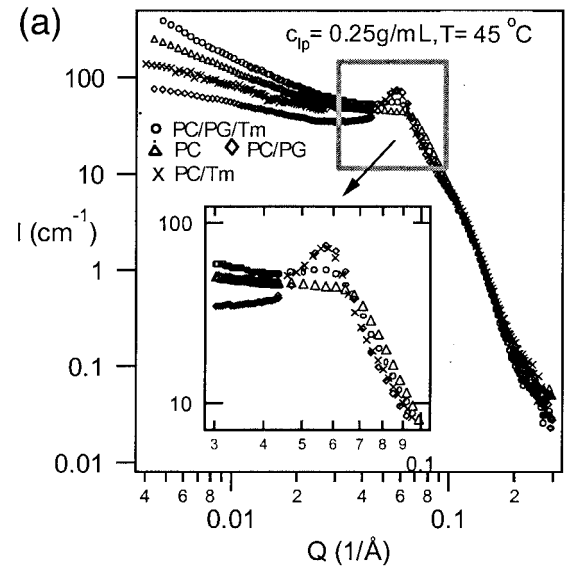

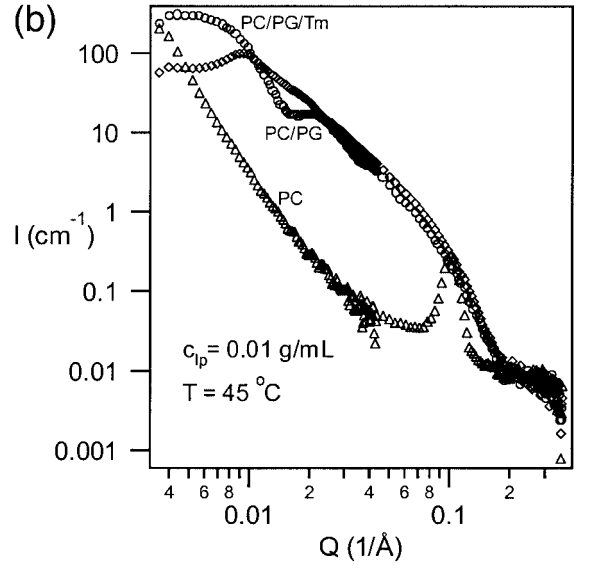

FIGURE 10 Comparison of SANS results for the PC, PC/PG, PC/PG/Tm, and PC/Tm (not included in *b*) series at 45°C for c_{lp} of 0.25 (*a*) and 0.01 g/ml (*b*). The inset in *a* zooms in on the data around the scattering peak to compare the sharpness of the peaks.

showed irregularly stacked, partially aligned bilayers (Bolze et al., 2000).

The formation of an L_2 phase, which yields a smaller and more regular interlamellar spacing, *D*, than the perforated lamellar phase, in some PC/PG samples (c_{lp} = 0.05 g/ml at 45°C) is not presently understood. We speculate that this smaller *D* could be due to an increased number of lamellae in solution possibly caused by the fragmentation of individ-

ual lamella due to the high charge density in PC/PG mixtures. For the PC/PG sample of c_{lp} = 0.01 g/ml, the increased D with increased T (Fig. 6 *b*) possibly results from the decreased number of particles in the system, implying that the bicellar disks aggregated into a certain larger morphology. This result is also consistent with the temperature-induced aggregation observed in the NMR experiments (Ottiger and Bax, 1998).

Increased charge density is also known to dampen the bilayer fluctuations resulting in more rigid lamellae (Higgs and Joanny, 1990). For this reason, MLVs, which have higher curvatures than the lamella does, appeared in the neutral PC mixtures, and ULVs were found in weakly charged PC/PG/Tm mixtures. Moreover, the negatively charged PC/PG bilayers are so rigid that even ULVs were not observed. Fig. 10 *b* demonstrates that the bilayer morphology can be dramatically different, even at the same c_{lp} (0.01 g/ml) and T (45°C), with changing surface charge density.

Another difference in the SANS data for the four lipid mixtures in Fig. 10 *a* is the slope and absolute intensity in the lower Q regime. Several factors may be the cause of this deviation such as the rigidity of the bilayer, the average size of the lamellae, and the existence of different structural domains. For the charged systems, the slope and absolute intensity seem to decrease with increased surface charge density, i.e., increased bilayer rigidity. Further study is needed to understand the influence of surface charge on the plateau region of the SANS profile.

The focus in this SANS study has been to explore the phase behavior of phospholipid mixtures, in the presence and absence of lanthanide ions, commonly used in NMR spectroscopic studies of membranes and membrane peptides and proteins (Sanders and Landis, 1995; Prosser et al. 1998b, 1999). The region of the phase diagram that is commonly exploited for purposes of preparing magnetically aligned NMR samples involves long-chain (DMPC and DMPG) and short-chain (DHPC) phospholipids in molar ratios of between 2.8 and 5, temperatures between 35°C and 45°C, and weight concentrations between 20% and 35%. ^{31}P and ^{2}H NMR studies of the constituent lipids definitively show that the long-chain phospholipids are arranged in bilayers, whereas the short-chain phospholipids exist in an environment with an isotropic curvature. However, the results of many studies, which speculate that bicelles possess a well-defined disk-shaped morphology, are in stark contrast with the results presented here and elsewhere (Nieh et al., 2001). Under the conditions, where macroscopic alignment is observed, our results suggest that the bilayers adopt a perforated lamellar structure. One of the earliest attempts to characterize bicelle morphology involved NMR diffusion measurements of water, using the pulsed-field gradient spin echo (PFGSE) technique (Chung and Prestegard, 1993). The authors successfully modeled the water diffusion as a stochastic jump process through a lattice of disk-shaped obstacles. Attempts to model the lattice as cylinders or as infinite sheets with holes did not reproduce the data. The PFGSE measurements depend on assumptions of bicelle size and morphology and on properties of bulk and surface water diffusion. Therefore, an unambiguous conclusion could not be made from this work alone. Subsequent small-angle x-ray scattering measurements revealed the bilayer thickness but did not substantiate the bicelle disk model (Hare et al., 1995). Vold and Prosser (1996) made use of deuterium NMR measurements of chain perdeuterated DHPC and DMPC lipids to assess bicelle morphology and size based on the ratio of C_2-methylene order parameters of the respective lipids. The measurements returned a size for the bicelles (e.g., a planar DMPC bilayer radius of 200 Å for a DMPC/DHPC = 3 bicelles) assuming the disk-shaped morphology. Though it was clear from this early NMR work that DHPC orientational order was further averaged by reorientation or fast lateral diffusion over a highly curved surface (such as the rim of a disk), this was also consistent with a magnetically aligned lamellar bilayer phase, perforated by DHPC-rich defect domains, whose radius of curvature is comparable to half the bilayer thickness. More recently, I. V. Shiyanovskaya, O. D. Lavrentovich, and R. S. Prosser (submitted for publication) have observed the lipid bilayer as a function of temperature and composition by polarized light microscopy. Their results reveal that the lipid mixtures are representative of a smectic or lamellar phase and not a nematic discoidal phase, which is consistent with our SANS results.

Now that the morphologies of a number of lipid mixtures as a function of temperature and lipid concentration have been identified, experiments that take advantage of this rich phase behavior can be designed. For instance, lamellae formed from PC/Tm or PC/PG/Tm mixtures can be used to study the structure of proteins aligned in such model biomembranes. Because the lamellae can be readily aligned in a magnetic field, it should be possible to measure the radii of gyration perpendicular and parallel to the membrane surface of integral, and perhaps even peripheral membrane proteins with SANS. Improved bilayer stacking, and better defined Bragg peaks, are apparently a partial consequence of a higher density of surface charge through the addition of lanthanides or negatively charged lipid. Contrast variation, achieved by adjusting the H_2O/D_2O ratio of the solution, can be used to enhance the scattering from the protein while minimizing that from the lipids. On the other hand, the MLV and ULV phases of the appropriate mixtures can be useful in the study of lipid/peptide or lipid/DNA complexes, which are of importance for drug or gene delivery. Contrast variation can again be used to separate the scattering of the lipid component from that of the DNA or peptide component, providing further insight into the structure and location of the DNA or peptide in the complex. Fast-tumbling bicellar disks now firmly established by small-angle neutron and light scattering, NMR, and other techniques (Luchette et al., 2002; Glover et al., 2001) are useful for high-resolution NMR studies of membrane peptides. The study

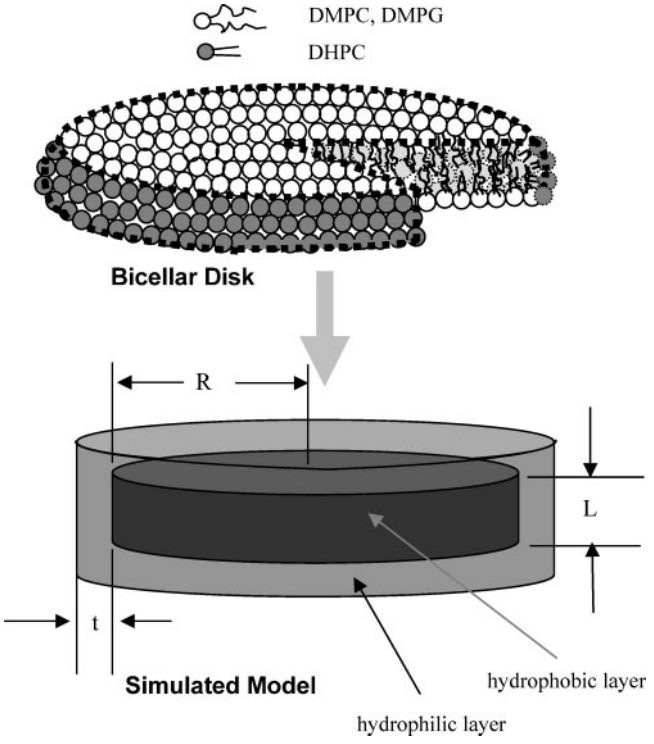

FIGURE 11 The bicellar disk model with short-chain lipids (DHPC) at the rim and long-chain lipids (DMPC or DMPG) at the top and bottom surfaces. The simplified model is a core-shell disk with the core (hydrophobic region) having radius *R*, and thickness *L*, and the hydrophilic shell having thickness *t*.

shows that this discoidal morphology can be obtained by varying not only *T* but also *q*.

Our characterization of scattering properties of these systems may lead to insights for improving the spectral resolution of solid-state NMR spectra of proteins in magnetically aligned lanthanide-doped media. Future studies of phase behavior of mixed lipid with a wide range of long- to short-chain phospholipid ratios and lipid concentrations may reveal other morphologies with useful applications.

APPENDIX

This section illustrates all the models for fitting our SANS data, and the resolution function for instrumental configurations is also taken into account during the fitting process. The SANS data were obtained by connecting two ranges of *Q* values with an overlapping regime from different instrumental configurations, which have different smearing effect. Thus, the fit intensities can be different at the same *q* in the overlapping regime due to this smearing effect resulting in the spikes on the best-fit curves in Figs. 1, 4, 6 *a*, and 7.

Bicellar discoidal model

In this model, the mixed lipid bilayered micelles are represented by randomly oriented uniform-sized disks with hydrophobic cores (radius being *R* and thickness being *L*) coated with hydrophilic shells of a uniform thickness, *t* as shown in Fig. 11. The scattering length density of each part is represented as the following: $\rho_{solvent}$ for the solvent, ρ_{core} for the core, and ρ_{shell} for the shell. For a dilute solution in which the interparticle interference can be ignored, the scattering function $I(Q)$ can be expressed as $\phi_{lipid}P_{disk}(Q)$, where ϕ_{lipid} is the volume fraction of the lipid mixtures and $P_{disk}(Q)$ is the scattering single form factor of the discoidal structure (Feigin and Svergun, 1987):

$$I(Q) = \phi_{lipid}P_{disk}(Q) = \phi_{lipid}\int_0^{\pi/2} \frac{g^2(Q,\alpha)}{V_{disk}} \sin\alpha d\alpha,$$

where

$$g(Q,\alpha) = 2(\rho_{core} - \rho_{shell})V_{core}\frac{\sin\left(\frac{QL}{2}\cos\alpha\right)}{\frac{QL}{2}\cos\alpha} \times \frac{J_1(QR\sin\alpha)}{QR\sin\alpha} + 2(\rho_{shell} - \rho_{solvent})V_{disk} \times \frac{\sin\left(Q\left(\frac{L}{2}+t\right)\cos\alpha\right)}{Q\left(\frac{L}{2}+t\right)\cos\alpha}\frac{J_1(Q(R+t)\sin\alpha)}{Q(R+t)\sin\alpha}, \quad \text{(A1)}$$

where $J_1(x)$ is the first-order Bessel function of x, and α is the angle between the bilayer normal, *n*, and *Q* for averaging over the orientations. The volumes for the core (V_{core}) and total disk (V_{disk}) can be calculated from *L*, *t*, and *R*. Fig. 1 shows the best fit to the SANS data for the PC/PG/Tm mixture at a c_{lp} of 0.0025 g/ml, which has the least interparticle interference. The scattering length densities were constrained to the calculated values ($\rho_{solvent} = 6.38 \times 10^{-6}$ Å^{-2} and $\rho_{core} = -4.3 \times 10^{-7}$ Å^{-2}) and literature values ($\rho_{shell} = 3.3 \times 10^{-6}$ Å^{-2}) (Nieh et al., 2001; Meuse et al., 1998) during the fitting. The dimensional parameters obtained from the best fit to the data were as follows: $R = 150 \pm 15$ Å, $L = 32 \pm 3$ Å, and $t = 8 \pm 1$ Å.

Infinite stacked lamellar model

In this model, bilayered lamellae are assumed to stack with their normals parallel with an average spacing, *D*, which has a Gaussian distribution with a standard deviation, σ_D. Therefore, the probability that the *n*th lamella lies at distance, *z*, along the lamellar normal direction is $w_n(z, D)$, which can be expressed as:

$$w_n(z, D) = \frac{1}{\sqrt{\pi n\sigma_D^2}} e^{-(z-nD)^2/\sigma_D^2} \quad \text{(A2)}$$

The structure factor, $S_{lam}(Q)$, for this infinitely stacking lamellae is the Fourier transform of $\Sigma_{n=-\infty}^{\infty} w_n(z,D)$ resulting in the following formula (Richter et al., 1997):

$$S_{lam}(Q) = \frac{\sinh(Q^2\sigma_D^2/4)}{\cosh(Q^2\sigma_D^2/4) - \cos(QD)} \quad \text{(A3)}$$

Each lamella represents a bilayer with a hydrophobic core of thickness, *L*, sandwiched between two hydrophilic layers of thickness, *t*. We consider the lamellae as flat disks with the radius, R_{lam}, which corresponds to the

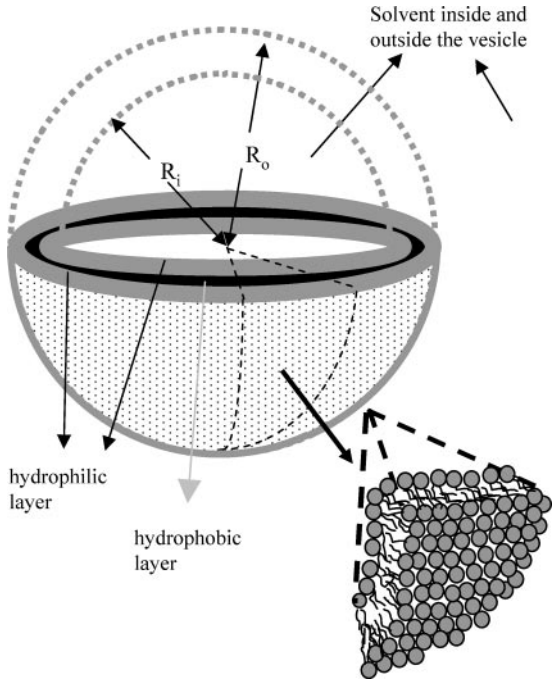

FIGURE 12 The unilamellar vesicles with inner and outer radii R_i and R_o, respectively. Solvent fills the inside and surrounds the outside the vesicle; the blow-up shows the detailed structure of the vesicle wall.

average persistence length on the lamellae. The larger R_{lam} is, the flatter is the lamellae. Then, the scattering function, $I(Q)$, can be expressed as Eq. 4, which incorporates the form factor for a single lamella with $S_{lam}(Q)$ while taking the spatial average over α, which is the angle between lamellar normal and scattering vector:

$$I(Q) = \phi_{lipid}\int_0^{\pi/2} \frac{g_{lam}{}^2(Q,\alpha)}{V_{lam}} S_{lam}(Q\cos\alpha)\sin\alpha d\alpha,$$

where

$$g_{lam}(Q,\alpha) = 2(\rho_{phob}-\rho_{phil})V_{phil}\frac{\sin\left(\frac{QL}{2}\cos\alpha\right)}{\frac{QL}{2}\cos\alpha} \times \frac{J_1(QR_{lam}\sin\alpha)}{QR_{lam}\sin\alpha} + 2(\rho_{phil}-\rho_{solventt})V_{lam} \times \frac{\sin\left(Q\left(\frac{L}{2}+t\right)\cos\alpha\right)}{Q\left(\frac{L}{2}+t\right)\cos\alpha}\frac{J_1(QR_{lam}\sin\alpha)}{QR_{lam}\sin\alpha}, \quad (A4)$$

where subscripts *phob*, *phil*, and *lam* represent hydrophobic, hydrophilic, and lamellae, respectively.

During the fitting procedure, the scattering length densities are constrained as described in the previous bicellar disk model, where $\rho_{solvent} = 6.38\times10^{-6}$ Å^{-2}, $\rho_{phob} = -4.3\times10^{-7}$ Å^{-2}, and $\rho_{phil} = 3.3\times10^{-6}$ Å^{-2}. The reasonable range for L is ~25 Å and t is ~8 Å in our previous study (Nieh et al., 2001). The parameters that are allowed to float freely during the fitting process are R_{lam}, D, and σ_D and are listed in Table 1. Good agreement between the fitting results (solid curves) and the data are shown in Figs. 4 and 6 *a*.

ULV model (including small MLV)

The scattering pattern of the ULV is derived from a spherical shell model as shown in Fig 12. Because $\rho_{solvent}$ is much higher than both ρ_{phil} and ρ_{phob}, the internal structure is not sensitive to variation in the SLD within the shell, the bilayer is simplified to have a uniform scattering length density, ρ_{lipid}, which is 3.2×10^{-7} Å^{-2} calculated from the molecular structure of the bilayer. The particle size distribution of the ULV was taken into account by using a Schulz distribution function, $f(r)$, with the polydispersity, p, defined as $\sigma/\langle R_o\rangle$, where σ^2 is the variance of vesicular outer radius, R_o and $\langle R_o\rangle$ is the average R_o. The scattering single form factor can be expressed as follows (Hayter, 1985):

$$P_{vesicle}(Q) = \frac{1}{V_{vesicle}}\int_0^\infty f(r)A_0^2(Qr)dr\,, \quad (A5)$$

where $V_{vesicle}$ is the total volume of a unilamellar vesicle, and

$$A_0(Qr) = \frac{4\pi(\rho_{lipid}-\rho_{solvent})}{Q^3}\left[\left(\sin Q\frac{R_i}{R_0}r - \sin Qr\right) - Qr\left(\frac{R_i}{R_0}\cos Q\frac{R_i}{R_0}r - \cos Qr\right)\right]$$

$$f(r) = \frac{(p^{-2/p^2})\left(\frac{r}{\langle R_0\rangle}\right)^{(1-p^2)/p^2} e^{-r/p^2\langle R_o\rangle}}{\langle R_0\rangle\Gamma\left(\frac{1}{p^2}\right)}$$

$\Gamma(1/p^2)$ is the gamma function and a reasonable value for p lies in the range of 0 and 1. R_i represents the inner radius of the ULV as $r = \langle R_o\rangle$. Fig. 7 shows the best-fitting result for a sample of PC/PG/Tm at $c_{lp} = 0.01$. The values for R_i and R_o were to be 154 ± 10 Å and 186 ± 10 Å, respectively, whereas for a sample with $c_{lp} = 0.0025$ g/ml, the best-fitting result for R_i and R_o was 68 ± 5 Å and 100 ± 10 Å, respectively.

As mentioned previously, the characteristic pattern of the ULV can be also observed in some small MLV systems if the outermost radius of the MLV is within the range of our SANS instrument. In the case of a PC mixture ($c_{lp} = 0.0025$ g/ml), the MLV peak at $Q = 0.097$ Å^{-1} appeared along with the scattering pattern corresponding to ULVs. This ULV model can be used to estimate the size of an MLV. The best-fitting result of the MLV R_o was 275 ± 10 Å as shown in Fig. 8 *c*.

This work is based upon activities supported by the National Science Foundation under agreement DMR 9986442.

REFERENCES

Bax, A., and N. Tjandra. 1997. High resolution heteronuclear NMR of human ubiquitin in an aqueous liquid crystalline medium. *J. Biomol. NMR.* 10:289–292.

Bolze, J., T. Fujisawa, T. Nagao, K. Norisada, H. Saito, and A. Naito. 2000. Small angle x-ray scattering and ^{31}P NMR studies on the phase behavior of phospholipid bilayered mixed micelles. *Chem. Phys. Lett.* 329:215–220.

Brunner, E., M. R. Arnold, W. Kremer, and. H. R. Kalbitzer. 2001. Pressure-stability of phospholipid bicelles: measurement of residual dipolar couplings under extreme conditions. *J. Biomol. NMR.* 21: 173–176.

Caffrey, M., J. Hogan, and A. Mencke. 1991. Kinetics of the barotropic ripple (P_β)/lamellar liquid crystal ($L\alpha$) phase transition in fully hydrated dimyristoyl phosphatidylcholine (DMPC) monitored by time-resolved x-ray diffraction. *Biophys. J.* 60:456–466.

Chung, J., and J. H. Prestegard. 1993. Characterization of field-oriented aqueous liquid crystals by NMR diffusion measurements. *J. Phys. Chem.* 97:9837–9843.

Feigin, L. A., and D. I. Svergun. 1987. Determination of the integral parameters of particles. *In* Structure Analysis by Small-Angle X-Ray and Neutron Scattering. G. W. Taylor, editor. Plenum Press, New York. 90–94.

Glinka, C. J., J. G. Barker, B. Hammouda, S. Krueger, J. J. Moyer, and W. J. Orts. 1998. The 30-m small-angle neutron scattering instruments at the National Institute of Standards and Technology. *J. Appl. Cryst.* 31:430–445.

Glover, K. J., J. A. Whiles, G. Wu, N.-J. Yu, R. Deems, J. O. Struppe, R. E. Stark, E. A. Komives, and R. R. Vold 2001. Structural evaluation of phospholipid bicelles for solution-state studies of membrane-associated biomolecules. *Biophys. J.* 81:2163–2171.

Hare, B. J., J. H. Prestegard, and D. M. Engelman. 1995. Small angle x-ray scattering studies of magnetically oriented lipid bilayers. *Biophys. J.* 69:1891–1896.

Hayter, J. B. 1985. Determination of structure and dynamics of micellar solutions by neutron small angle scattering. *In* Physics of amphiphiles: micelles, vesicles, and microemulsions. V. Degiorgio and M. Corti, editors. Elsevier Science, Amsterdam. 60–93.

Higgs, P. G., and J.-F. Joanny. 1990. Enhanced membrane rigidity in charged lamellar phases. *J. Phys. France.* 51:2307–2320.

Katsaras, J., R. L. Donaberger, I. P. Swainson, D. C. Tennant, Z. Tun, R. R. Vold, and R. S. Prosser. 1997. Rarely observed phase transitions in a novel lyotropic liquid crystal system. *Phys. Rev. Lett.* 78:899–902.

Laggner, P. 1994. X-ray diffraction on biomembrane with emphasis on lipid moiety. *In* Subcellular Biochemistry: Physicochemical Methods in the Study of Biomembranes. H. J. Hilderson and G. B. Ralston, editors. Plenum Press, New York. 451–492.

Lohner, K., E. Staudegger, E. J. Prenner, R. N. A. H. Lewis, M. Kriechbaum, G. Degovics, and R. N. McElhaney. 1999. Effect of staphylococcal δ-lysin on the thermotropic phase behavior and vesicle morphology of dimyristoyl phosphatidylcholine lipid bilayer model membranes: differential scanning calorimetric, ^{31}P nuclear magnetic resonance and Fourier transform infrared spectroscopic, and x-ray diffraction studies. *Biochemistry.* 38:16514–16528.

Losonczi, J. A., and J. H. Prestegard. 1998. Improved dilute bicelle solutions for high resolution NMR of biological macromolecules. *J. Biomol. NMR.* 12:447–451.

Luchette, P. A., T. N. Vetman, R. S. Prosser, R. E. W. Hancock, M.-P. Nieh, C. J. Glinka, S. Krueger, and J. Katsaras. 2002. Morphology of fast-tumbling bicelles: a small angle neutron scattering and NMR study. *Biochim. Biophys. Acta.* 1513:83–94.

Meuse, C. W., S. Krueger, C. F. Majkrzak, J. A. Dura, J. Fu, J. T. Connor, and A. Plant. 1998. Hybrid bilayer membrane in air and water: infrared spectroscopy and neutron reflectivity studies. *Biophys. J.* 74:1388–1398.

Nieh, M.-P., C. J. Glinka, S. Krueger, R. S. Prosser, and J. Katsaras. 2001. SANS study of structural phases of magnetically alignable lanthanide-doped phospholipid mixtures. *Langmuir.* 17:2629–2638.

Ottiger, M., and A. Bax. 1998. Characterization of magnetically oriented phospholipid micelles for measurement of dipolar couplings in macromolecules. *J. Biomol. NMR.* 12:361–372.

Prosser, R. S., H. Bryant, R. G. Bryant, and R. R. Vold. 1999. Lanthanide chalets as bilayer alignment tools in NMR studies of membrane-associated peptides. *J. Magn. Reson.* 141:256–260.

Prosser, R. S., S. A. Hunt, J. A. DiNatale, and R. R. Vold. 1996. Magnetically aligned membrane model systems with positive order parameter: switching the sign of S_{zz} with paramagnetic ions. *J. Am. Chem. Soc.* 118:269.

Prosser, R. S., J. S. Hwang, and R. R. Vold. 1998a. Magnetically aligned phospholipid bilayers with positive ordering: a new model membrane system. *Biophys. J.* 74:2405–2418.

Prosser, R. S., V. B. Volkov, and I. V. Shiyanovskaya. 1998b. Solid-state NMR studies of magnetically aligned phospholipid membranes: taming lanthanides for membrane protein studies. *Biochem. Cell Biol.* 76: 443–451.

Prosser, R. S., V. B. Volkov, and I. V. Shiyanovskaya. 1998c. Novel chalet-induced magnetic alignment of biological membranes. *Biophys. J.* 75:2163–2169.

Raffard, G., S. Steinbruckner, A. Arnold, J. H. Davis, and E. J. Dufourc. 2000. Temperature-composition diagram of dimyristoyl phosphatidylcholine-dicaproyl phosphatidylcholine "bicelles" self-orienting in the magnetic field: a solid state ^2H and ^{31}P NMR study. *Langmuir.* 16: 7655–7662.

Richter, D., D. Schneiders, M. Monkenbusch, L. Willner, L. J. Fetters, J. S. Huang, M. Lin, K. Mortensen, and B. Farago. 1997. Polymer aggregation with crystalline cores: the system polyethylene-poly(ethylenepropylene). *Macromolecules.* 30:1053–1068.

Sanders, C. R. II., B. J. Hare, K. P. Howard, and J. H. Prestegard. 1994. Magnetically-oriented phospholipid micelles as a tool for the study of membrane-associated molecules. *Prog. NMR Spectrosc.* 26:421–444.

Sanders, C. R. II, and G. C. Landis. 1994. Facile acquisition and assignment of oriented sample NMR spectra for bilayer surface-associated protein. *J. Am. Chem. Soc.* 116:6470–6471.

Sanders, C. R. II, and G. C. Landis. 1995. Reconstitution of membrane-proteins into lipid-rich bilayered mixed micelles for NMR studies. *Biochemistry.* 34:4030–4040.

Sanders, C. R. II, and R. S. Prosser. 1998. Bicelles: a model membrane system for all seasons? *Structure.* 6:1227–1234.

Sanders, C. R. II., and J. Schwonek. 1992. Characterization of magnetically orientable bilayers in mixtures of dihexanoyl phosphatidylcholine and dimyristoyl phosphatidylcholine by solid-state NMR. *Biochemistry.* 31: 8898–8905.

Sternin, E., D. Nizza, and K. Gawrisch. 2001. Temperature dependence of DMPC/DHPC mixing in a bicellar solution and its structural implications. *Langmuir.* 17:2610–2616.

Struppe, J., and R. R. Vold. 1998. Dilute bicellar solutions for structural NMR work. *J. Magn. Reson.* 135:541–546.

Ulrich, A. S., and A. Watts. 1993. H-2 NMR lineshapes of immobilized uniaxially oriented membrane-proteins. *Solid State Nuclear Magn.* 2:21–36.

Vold, R. R., and R. S. Prosser. 1996. Magnetically oriented phospholipid bilayered micelles for structural studies of polypeptides. Does the ideal bicelle exist? *J. Magn. Reson. B.* 113:267–271.

Vold, R. R., R. S. Prosser, and A. J. Deese. 1997. Isotropic solutions of phospholipid bicelles: a new membrane mimetic for high resolution NMR studies of polypeptides. *J. Biomol. NMR.* 9:329–355.